A combined modeling and multipectral/multiresolution remote sensing approach for disaggregation of surface soil moisture: Application to SMOS configuration

Olivier Merlin, Ghani Chehbouni, Yann H. Kerr, E.G. Njoku, D. Entekhabi

To cite this version:

Olivier Merlin, Ghani Chehbouni, Yann H. Kerr, E.G. Njoku, D. Entekhabi. A combined modeling and multipectral/multiresolution remote sensing approach for disaggregation of surface soil moisture: Application to SMOS configuration. IEEE Transactions on Geoscience and Remote Sensing, 2005, 43 (9), pp.2036-2050. 10.1109/tgrs.2005.853192 . ird-00390484

HAL Id: ird-00390484
https://ird.hal.science/ird-00390484v1

Submitted on 2 Jun 2009

A Combined Modeling and Multi-Spectral/Multi-Resolution Remote Sensing Approach for Disaggregation of Surface Soil Moisture: Application to SMOS Configuration

Olivier Merlin, Abdel G. Chehbouni, Yann H. Kerr, *Senior Member, IEEE,*
Eni G. Njoku, *Fellow, IEEE,* and Dara Entekhabi, *Member, IEEE*

Abstract

A new physically-based disaggregation method is developed to improve the spatial resolution of the surface soil moisture extracted from the Soil Moisture and Ocean Salinity (SMOS) data. The approach combines the 40 km resolution SMOS multi-angular brightness temperatures and 1 km resolution auxiliary data composed of visible, near-infrared and thermal infrared remote sensing data and all the surface variables involved in the modeling of land surface-atmosphere interaction available at this scale (soil texture, atmospheric forcing, etc.). The method successively estimates a relative spatial distribution of soil moisture with fine scale auxiliary data, and normalizes this distribution at SMOS resolution with SMOS data. The main assumption relies on the relationship between the radiometric soil temperature inverted from the thermal infrared and the microwave soil moisture. Based on synthetic data generated with a land surface model, it is shown that the radiometric soil temperature can be used as a tracer of the spatial variability of the 0–5 cm soil moisture. A sensitivity analysis shows that the algorithm remains stable for big uncertainities in auxiliary data and that the uncertainity in SMOS observation seems to be the limiting factor. Finally, a simple application to the SGP97/AVHRR data illustrates the usefullness of the approach.

Index Terms

Surface soil moisture, disaggregation, SMOS mission, multi-spectral remote sensing, synergy.

The authors are grateful for funding from the CNES program “Programme Atmosphère Océan Biosphère”.

A Combined Modeling and Multi-Spectral/Multi-Resolution Remote Sensing Approach for Disaggregation of Surface Soil Moisture: Application to SMOS Configuration

I. INTRODUCTION

Soil moisture is a key hydrological variable that plays an important role in land surface-atmosphere interactions. By controlling the partition of rainfall into runoff and infiltration and available energy at the surface into sensible and latent heat flux, soil moisture plays a crucial role in boundary layer development and therefore in climate modeling at both regional and global scale.

Microwave satellite sensors have proven to be effective for soil moisture sensing because of the large contrast between the dielectric properties of liquid water (80) and those of dry soil (4). This results in a wide range of values for the soil-water mixture (4-40) which impact the natural microwave emission from the soil. In particular, sensors operating at low frequencies (L-Band) such as PBMR, ESTAR have been found to be very effective in inferring surface soil moisture at different space-time scales [1]–[4].

The Soil Moisture and Ocean Salinity (SMOS) mission [5] has been recently selected by the European Space Agency (ESA) and it is scheduled for launch in 2007. This L-band radiometer is based on an innovative two-dimensional aperture synthesis concept. This sensor has new and significant capabilities in terms of multi-angular viewing configurations. This allows for simultaneously retrieving the 0–5 cm soil moisture and vegetation biomass [6] with a sampling cycle ranging from 1 to 3 days and a mean ground resolution (pixel size) of about 40 km. This instrument will then provide the much needed global data set of soil moisture and other surface variables to be implemented in general circulation and climate models.

At regional scale, recent efforts have been dedicated towards the improvement of the modeling of land surface-atmosphere interaction through a three-dimensional representation of hydrological processes by incorporating more realistic land-surface schemes and spatial information such as surface soil moisture from remote sensing [7]. The use of SMOS data with its 40 km resolution in such hydrological models is not straightforward. The scale at which most hydrological processes (runoff, infiltration, evapotranspiration, etc.) should be captured for improving the understanding and subsequently the representation of surface processes in regional models is of about 1 to 10 km [8]–[11].

To overcome this difficulty, different approaches have been recently adopted to distribute fine scale soil moisture within passive microwave pixels. For example, Pellenq et al. (2003) [12] coupled a Soil Vegetation Atmosphere Transfer (SVAT) model to distributed hydrological formalism. Lumped values of soil moisture were then disaggregated using simple relationships between mean values, local topography and soil depth information. A different approach was proposed by Kim and Barros (2002) [13] who showed that the space-time structure of soil moisture fields can be statistically explained by the scaling behavior of auxiliary data such as topography, soil texture, vegetation water content and rainfall. Based on these findings, they [14] developed time-varying linear combinations of the spatial distributions of relevant auxiliary data to interpolate coarse resolution soil moisture. The so-called 4-D variational data assimilation scheme was used by Reichle et al. (2001) [15] to estimate soil moisture values at the scale of one fourth the resolution of microwave data. Bindlish and Barros (2002) [16] combined active-passive microwave remote sensing to interpolate the coarse resolution brightness temperature. The downscaled brightness temperatures were then used to retrieve soil moisture estimates at the scale of active microwave data. Similarly, Chauhan et al. (2003) [17] used linear regressions between a vegetation index, surface temperature and soil moisture. By aggregating the vegetation index and surface temperature, a linkage model was developed at the scale of the microwave observation, and then applied at fine scale to disaggregate microwave soil moisture into high-resolution soil moisture.

The objective of the paper is to develop a new physically-based disaggregation method to improve the spatial resolution of the surface soil moisture extracted from SMOS. The approach is based on an original combination of the 40 km resolution SMOS multi-angular brightness temperatures and 1 km resolution auxiliary data composed of visible, near-infrared and thermal infrared remote sensing data and all the surface variables involved in the modeling of land surface-atmosphere interaction available at this scale (soil texture, atmospheric forcing, etc.). The approach for disaggregating SMOS soil moisture involves two steps. First, the disaggregated soil moisture is expressed as function of the radiometric soil temperature derived from fine scale auxiliary data, and two parameters defined at SMOS scale. The two parameters are the SMOS scale soil moisture and a parameter fixing the range covered by disaggregated values. The second step consists of inverting both parameters from SMOS data.

We begin in section II by presenting the models used and describing the main steps of the method. In section III, we list the assumptions implicitely made in the development of the method. These assumptions are first checked in section IV with a synthetic scene representing a heterogeneous SMOS pixel. In section V, the robustness of the disaggregation method is tested by generating a specified noise to be added to the synthetic input dataset. In section VI, the disaggregation method is applied to the data collected during the 1997 Southern Great Plains Hydrology Experiment and the data of AVHRR channels 1, 2, 4 and 5. In the final section, we summarize the different results of the paper and we discuss about the applicability of such a disaggregation scheme on an operational basis.

The results presented in this paper are mostly based on synthetic data generated with physically-based models to evaluate the approach. We underline the fact that using synthetic data does not allow us to address a number a complications that will be encountered in operational settings.

II. METHOD

A disaggregation method of the 40 km resolution SMOS soil moisture is developed in this section. The three models used are first presented before we describe the main steps of the method.

A. Models

The disaggregation method uses three models: an L-band radiative transfer model, a thermal infrared radiative transfer model and a land surface model. In this section, the three models are described and the consistency between the different surface variables involved is discussed.

1) L-band radiative transfer model: a radiative transfer model at L-band (RT model) is used to simulate the angular and bi-polarized SMOS brightness temperatures. A complete description is given in [6]. Using the tau-omega formalism [18]–[20] and neglecting atmospheric effects, the L-band brightness temperature $TB(\theta, p)$ at the incidence angle θ and at

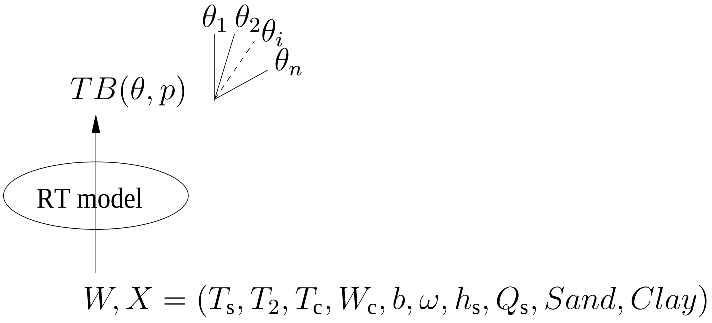

Fig. 1. Schematic diagram showing the input/output data of the L-band radiative transfer (RT) model. The input are: the 0–5 cm soil moisture W, the soil surface temperature T_{s}, the deep soil temperature T_2, the canopy temperature T_{c}, the vegetation water content W_{c}, the so-called b parameter of vegetation, the single-scattering albedo of the canopy ω, the roughness parameter h_{s}, the polarization-mixing parameter Q_{s} and the soil texture composed of sand and clay fractions. The ouput is a vector noted TB of bi-polarized and multi-angular brightness temperatures. It is composed of $2n$ independent brightness temperatures.

polarization p (H or V) can be expressed as:

$$TB(\theta,p) = T_{\text{e}} e_p(\theta,p) \text{exp}(-\tau/\text{cos}\theta) + T_{\text{c}}(1-\omega)[1-\text{exp}(-\tau/\text{cos}\theta)][1+r_p(\theta,p)\text{exp}(-\tau/\text{cos}\theta)] \tag{1}$$

with T_{e} the effective soil temperature, T_{c} the canopy temperature, e_p the soil emissivity, r_p the soil reflectivity (related to the soil emissivity by $r_p = 1 - e_p$), τ the nadir optical depth of the canopy and ω the single-scattering albedo of the canopy. The parameterization of [21] is used to compute the effective soil temperature T_{e} as function of the deep soil temperature T_2 (approximately at 50 cm) and the soil surface temperature T_{s} (approximately corresponding to a depth interval of 0–5 cm). The soil microwave emissivity e_p for polarization p is calculated from the soil dielectric permittivity parameterized with soil texture [22] and from the incidence angle θ using the Fresnel equations. The soil roughness is accounted for using the simple approach of [23] based on the roughness parameter h_{s} and the polarization-mixing parameter Q_{s}. At L-band, the single-scattering albedo of the canopy is small (we took 0.05 for both polarizations). The nadir optical depth τ is related to the vegetation water content W_{c} by $\tau = bW_{\text{c}}$ [24]. The input data of RT model are listed in the schematic diagram of Fig. 1 where W is the 0–5 cm soil moisture and $Sand$ and $Clay$ are the sand and clay fraction of soil. The output of RT model is a vector TB of bi-polarized and multi-angular brightness temperatures.

2) Thermal infrared radiative transfer model: a radiative transfer model in the thermal infrared (RT-TIR model) is used to invert the radiometric soil temperature from bi-directional radiometric surface temperature [25]–[31]. Assuming surface emissivity is close to 1, the radiometric surface temperature $T_{\text{rad}}(\theta)$ at angle θ is simply computed as:

$$T_{\text{rad}}(\theta) = \big[1 - f_{\text{c}}(\theta)\big] T_{\text{s}} + f_{\text{c}}(\theta) T_{\text{c}} \tag{2}$$

with T_{s} the radiometric effective soil (the mixture of sunlit and shadowed soil) temperature, T_{c} the radiometric effective canopy (the mixture of sunlit and shadowed canopy) temperature and $f_{\text{c}}(\theta)$ the angular fractional vegetation cover. The inversion of component temperatures (i.e. the radiometric soil temperature and the radiometric canopy temperature) requires the radiometric surface temperature at two distinct angles $T_{\text{rad}}(\theta_1)$ and $T_{\text{rad}}(\theta_2)$ and the viewing angle-dependent vegetation fraction which can be estimated using visible and near infrared data at the same resolution. Following [32], the fractional vegetation cover $f_{\text{c}}(\theta)$ at angle θ can be obtained with the semi-empirical model:

$$f_{\text{c}}(\theta) = 1 - \left(\frac{NDVI_{\text{max}}(\theta) - NDVI(\theta)}{NDVI_{\text{max}}(\theta) - NDVI_{\text{min}}(\theta)} \right)^p \tag{3}$$

where $NDVI_{\text{min}}(\theta)$ is the bare soil NDVI, $NDVI_{\text{max}}(\theta)$ the NDVI at 100%, and p the ratio of a leaf angle distribution term to a canopy extinction term. The input/ouput data of RT-TIR model in the inverse mode are shown in Fig. 2.

Note that the second Along-Track Scanning Radiometer (ATSR-2) on board the European Remote Sensing satellite is a possible source of bi-angular thermal infrared data. This instrument is currently able to provide quasi-simultaneous multispectral (from visible to thermal infrared) measurements at two view angles (approximately 0 and 53 at surface).

3) Land surface model: a land surface (LS) model is used to simulate the radiometric soil temperature under differerent surface conditions within the SMOS pixel. A complete description is provided in [33]. Briefly, the soil is divided into a top soil layer on which soil evaporation depends and a deep layer which mainly controls vegetation transpiration. The top soil layer is characterized by a resistance to evaporation which depends on surface soil moisture W. Similarly, the deep soil layer is characterized by its soil water content W_2 used in the parameterization of stomatal control on transpiration. The surface is described according to the two-layer formalism of [34]. LS model solves two different energy balance equations from which soil and vegetation temperatures are derived through an iterative scheme. The atmospheric variables are solar radiation S, air temperature T_{a}, air relative humidity q_{a} and wind velocity u_{a} at a reference height. The vegetation characteristics used as inputs are the leaf area index LAI and the canopy height h_{c}. Soil textural properties are derived from sand

and clay fractions as in [35], [36]. The input data of LS model are listed in the schematic diagram of Fig. 2. The output of interest as it is shown in the development of the method is the radiometric soil temperature $T_{\rm s}$.

4) Consistency between models: the three models presented above were chosen so that the different surface variables involved be consistent between them. In particular, the 0–5 cm microwave soil moisture involved in RT model is consistent with the 0–5 cm surface soil moisture of the top layer of LS model. Similarly, the radiometric soil temperature inverted with RT-TIR model has precisely the same definition as the top soil temperature simulated by LS model. In LS model, the temperature of the top soil layer is indeed used to compute the net radiation of soil. Note that the soil surface temperature involved in RT model, which corresponds approximately to a depth interval of 0–5 cm is not perfectly consistent with the 1 mm radiometric soil temperature involved in models RT-TIR and LS. However, as RT model ponders the soil surface temperature with the deep soil temperature to compute the microwave effective soil temperature, the authors consider that the radiometric soil temperature $T_{\rm s}$ is a good approximation of the integrated 0–5 cm soil temperature as input of RT model.

B. Disaggregation Method

The disaggregation of the soil moisture extracted from SMOS data involves two successive steps. In a first step, auxiliary data at 1 km resolution are used to describe the spatial variability of surface soil moisture within the 40 km resolution SMOS pixel. In a second step, the relative distribution of surface soil moisture obtained in step 1 is normalized at SMOS scale with SMOS observation.

In step 1, it is assumed that the radiometric soil temperature inverted from dual-angle measurement in the thermal infrared [25], [31] can provide some information about the spatial variability of surface soil moisture [29], [30]. By linking at first order the disaggregated soil moisture to the inverted radiometric soil temperature, a relative soil moisture distribution depending on two SMOS scale parameters is expressed. In step 2, the normalization of the relative distribution consists of calibrating both parameters by linking the soil moisture distribution to SMOS observation via RT model.

Both steps are conceptually equivalent to the method developed by Sivapalan [37] to disaggregate water storage within a landscape. In that study, the spatial variability of local water storage was expressed as a function of a local topographic index. Local water storage was then a function of two parameters defined at the scale of the hillslope: a parameter f_0

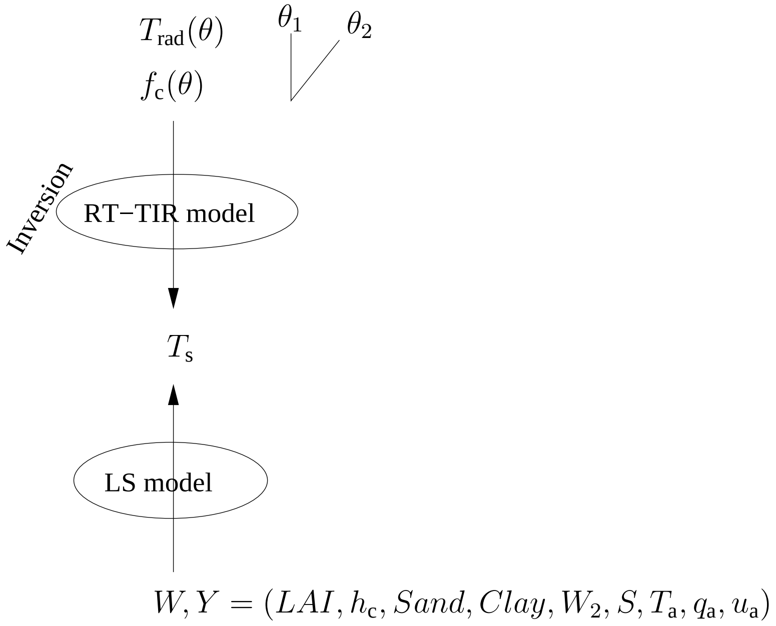

Fig. 2. Schematic diagram showing the input/output data of the radiative transfer model in the thermal infrared (RT-TIR model) and the input/output data of the land surface (LS) model. RT-TIR model is used in the inverse mode to invert the radiometric soil temperature T_{s} from the radiometric surface temperature at two distinct angles $T_{\mathrm{rad}}(\theta_1)$ and $T_{\mathrm{rad}}(\theta_2)$. The inversion of T_{s} requires the directional fractional vegetation cover obtained with optical data at both angles $f_{\mathrm{c}}(\theta_1)$ and $f_{\mathrm{c}}(\theta_2)$. LS model is used to simulate the radiometric soil temperature T_{s} under different surface conditions within the SMOS pixel. The input are: LAI, the canopy height h_{c}, the soil texture composed of sand and clay fractions, the deep soil moisture W_2, the solar radiation S, the air temperature T_{a}, the relative humidity of air q_{a} and the wind velocity u_{a}.

controlling the mean level of water storage and a parameter f_1, called the contrast parameter, fixing the range covered by local values within the landscape. In a second step, one parameter (f_0) of the water storage distribution was calibrated comparing the average of distributed values to the value measured at the scale of the hillslope.

However, an essential difference between the disaggregation of SMOS data and the study case of Sivapalan [37] is that the available information at regional scale is multiple in our case. As it shown in the development of the method, the fact that each SMOS observation is composed of multi-angular/multi-independent brightness temperatures allows to calibrate simultaneously both parameters f_0 and f_1.

The two main steps of the disaggregation method (i.e. estimate a relative distribution, and normalize the relative distribution) are described below and shown in Fig. 3.

1) Estimate a relative soil moisture distribution: the typical resolution of 1 km that is currently obtained in the thermal infrared and the correlation between the radiometric surface temperature and the soil water content makes the radiometric surface temperature useful for disaggregation purposes [17]. The point is that the link between the remotely sensed radiometric surface temperature T_{rad} and the microwave near-surface soil moisture W is relativelly indirect and is function of the surface conditions that are likely to vary in space. In particular, the spatial variability of vegetation cover (and soil texture, atmospheric conditions, etc.) at the scale of 1 km may induce a systematic noise on the relationship between T_{rad} and W. To account for both difficulties, the disaggregation method successively inverts the radiometric soil temperature T_{s} which is more directly related to W than T_{rad} and extracts specifically the information on W that is contained in T_{s} using LS model and the available information on the surface conditions within the SMOS pixel.

a) Invert the radiometric soil temperature T_s: the correlation between the radiometric surface temperature and near-surface soil moisture can be explained by the surface thermal inertia concept. The surface thermal inertia is affected by soil water content with two distinct bio-physical processes: the evaporation at soil level of the near-surface soil moisture and the transpiration at plant level of the root-zone soil moisture. Both phenomena tends to counter synergistically the increase of component temperatures, and therefore the radiometric surface temperature. However, the near-surface soil temperature over a vegetated surface is more related to the near-surface soil moisture and the vegetation temperature is more related to the root-zone soil moisture [29], [30]. It follows that the near-surface soil temperature is more valuable than the radiometric surface temperature for disaggregation purposes of the 0–5 cm microwave soil moisture. As a matter of fact, the disaggregation method uses the soil temperature rather than the radiometric surface temperature. Given that the 0–5 cm soil temperature is not observed in the thermal infrared, the 1 mm radiometric soil temperature is assumed to be inverted from bi-angular thermal infrared data as shown before in Section II.A.2..

Note that the inversion of the radiometric soil temperature is a necessary step of the disaggregation method. We underline the fact that the disaggregation method cannot be used in the regions where the robustness of the inversion process of the radiometric soil temperature T_{s} is poor (e.g. areas with relatively high vegetation cover).

b) Extract the information contained in T_s: the disaggregation strategy is based on the spatial correlation between surface soil moisture and the remotely sensed radiometric soil temperature. One difficulty to link surface soil moisture to the radiometric soil temperature is the dependence of the radiometric soil temperature to the variables contained in the vector Y of Fig. 2 (e.g. LAI, soil texture, atmospheric forcing). To overcome this difficulty, the method simulates the variability of the radiometric soil temperature that is specifically due to the variables contained in Y. In practice, two radiometric soil temperatures are simulated with LS model. First, LS model is used to simulate the radiometric soil temperature noted $T_{\mathrm{s}l}$ (index $_l$ refers to local scale) associated with the measured local surface conditions Y_l^m (exponent ^{m} refers to a measured or known variable):

$$T_{\mathrm{s}l} = \mathbf{LS}(W_l, Y_l^m) \tag{4}$$

Second, LS model is used to simulate the radiometric soil temperature noted $\overline{T_{\mathrm{s}l}}$ associated with the surface conditions aggregated at the scale of the SMOS pixel Y_G (index $_G$ refers to SMOS resolution or global scale):

$$\overline{T_{\mathrm{s}l}} = \mathbf{LS}(W_l, Y_G) \tag{5}$$

where Y_G is computed averaging the local surface conditions Y_l^m over the SMOS pixel:

$$Y_G(i) = \frac{1}{N}\sum_{l=1}^{N} Y_l^m(i) \tag{6}$$

with N the number of sub-pixels contained in the SMOS pixel ($40 \times 40 = 1600$ in our case). The difference $(T_{\mathrm{s}l} - \overline{T_{\mathrm{s}l}})$ represents the predicted contribution of the radiometric soil temperature that is due to the varibility of Y_l within the SMOS pixel. By substracting $(T_{\mathrm{s}l} - \overline{T_{\mathrm{s}l}})$ to the measured radiometric soil temperature $T_{\mathrm{s}l}^m$, we obtain a theoretical variable called Projected soil temperature $\overline{T_{\mathrm{s}l}^m}$ and formally defined by:

$$\overline{T_{\mathrm{s}l}^m} = T_{\mathrm{s}l}^m - (T_{\mathrm{s}l} - \overline{T_{\mathrm{s}l}}) \tag{7}$$

By definition, the spatial variability of Projected soil temperature is attributed uniquely to the spatial variability of near-surface soil moisture. The disaggregation method can therefore use $\overline{T_{\mathrm{s}l}^m}$ to explain the spatial variability of W_l.

c) Estimate a relative spatial distribution: a relative spatial distribution of soil moisture is expressed by linking the disaggregated soil moisture W_l to Projected soil temperature $\overline{T_{\mathrm{s}l}^m}$ at first order:

$$W_l = f_0 + f_1 \overline{T_{\mathrm{s}l}^m} \tag{8}$$

with f_0 and f_1 two parameters defined at SMOS scale.

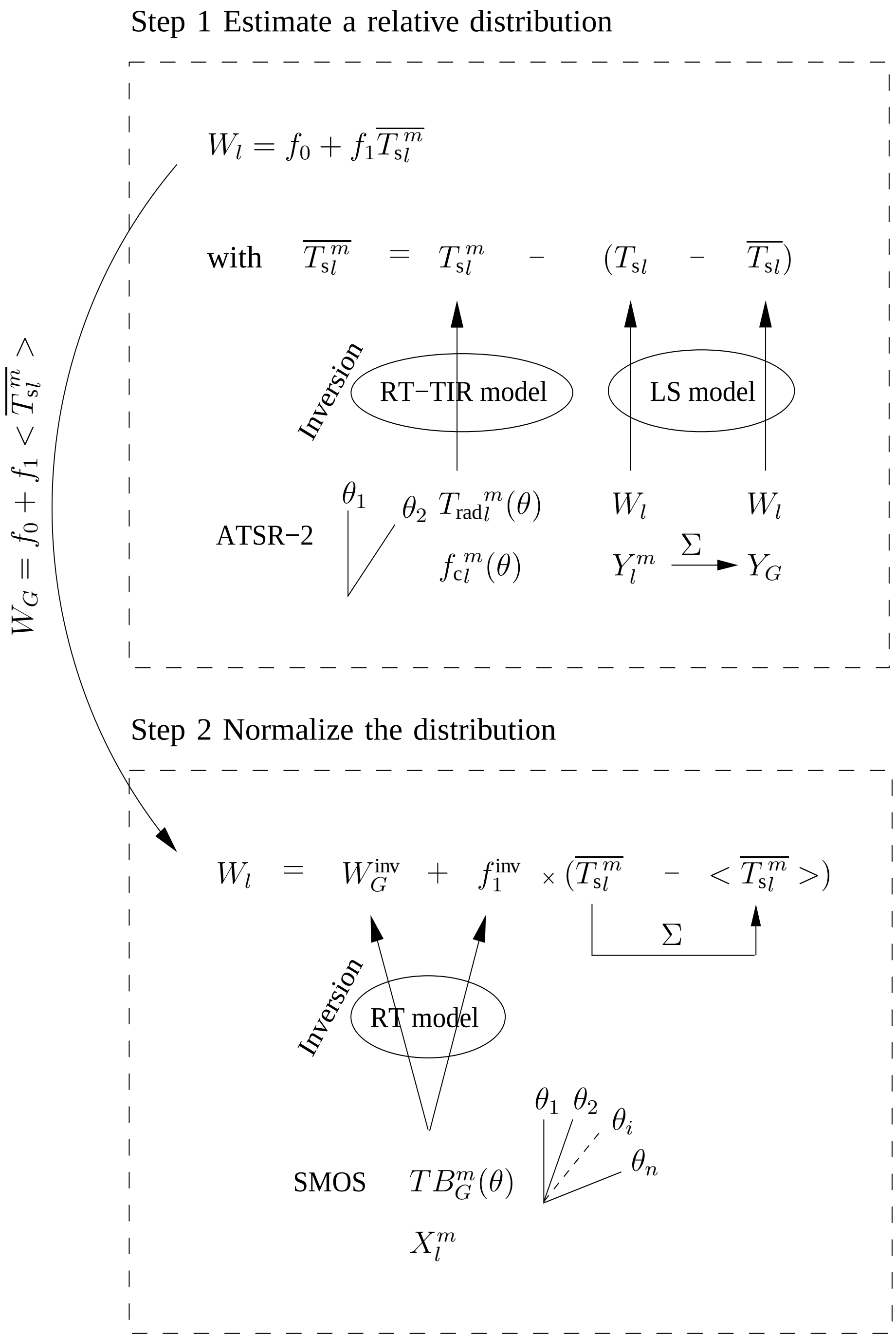

Fig. 3. The two successive steps of the method are presented. In step 1, a relative spatial distribution of soil moisture is estimated from the radiometric soil temperature T_{sl}^m inverted with RT-TIR model and from LS model predictions giving the contribution of the radiometric soil temperature due to surface conditions' heterogeneity $(T_{sl} - \overline{T_{sl}})$. The disaggregated soil moisture is then a function of two SMOS scale parameters f_0 and f_1. In step 2, the local relationship derived in step 1 is rewritten at global scale to make the SMOS scale soil moisture W_G appear in the expression. Both parameters W_G and f_1 are then inverted from SMOS data to normalize the distribution.

2) Normalize the relative distribution: in the second step of the disaggregation method, the relative soil moisture distribution of (8) is normalized at the scale of the SMOS pixel. The normalization consists of using the multi-angular SMOS observation to calibrate parameters f_0 and f_1.

From a theoretical point of view, the calibration of f_0 and f_1 can be compared to the inversion process used by the SMOS mission. As explained in [6] the approach of SMOS is based on the use of the multi-angular/multi-independent SMOS observation to infer simultaneously soil moisture and vegetation water content. Although f_0 and f_1 are abstract parameters, our approach is similar to [6] because f_0 and f_1 are both defined at the scale of the SMOS pixel as well as SMOS soil moisture and SMOS vegetation water content. In fact, the key to the calibration of the couple (f_0, f_1) is double: (i) the L-band angular signature of a SMOS pixel depends on both f_0 and f_1 and (ii) the SMOS observation is composed of multi-angular (at least two independent) brightness temperatures.

In practice, the normalization of the relative distribution of (8) is performed by looking for a particular solution of the couple (f_0, f_1) such that the SMOS scale soil moisture W_G appears in the expression of W_l. Both parameters W_G and f_1 are then inverted by matching the SMOS observation simulated from the disaggregated soil moisture and the measured SMOS observation.

a) Find a particular solution: we look for a particular solution of the couple (f_0, f_1) to make the SMOS scale soil moisture W_G appear in the expression of the disaggregated soil moisture. Let f_0 such as:

$$f_0 = W_G - f_1 < \overline{T_{\mathrm{s}l}^{m}} > \tag{9}$$

where $< \overline{T_{\mathrm{s}l}^{m}} >$ is the Projected soil temperature aggregated (linearly) over the SMOS pixel.

b) Express the disaggregated soil moisture: replacing f_0 in (8) by the expression of (9), we obtain a new expression of the disaggregated soil moisture, which is now a function of the couple (W_G, f_1):

$$W_l(W_G, f_1) = W_G + f_1(\overline{T_{\mathrm{s}l}^{m}} - < \overline{T_{\mathrm{s}l}^{m}} >) \tag{10}$$

In this expression, we clearly see the function of each parameter: W_G parameter determines the effective level of the distribution at SMOS scale whereas the contrast parameter of the distribution f_1 fixes the range covered by disaggregated values.

c) Build a cost function: a cost function is built in order to evaluate the distance between the SMOS observation simulated from the disaggregated soil moisture of (10) and the measured SMOS observation. The cost function F is defined as:

$$F(W_G, f_1) = \left\| \frac{1}{N} \sum_{l=1}^{N} \mathbf{RT}\big(W_l, X_l^m\big) - TB_G^m \right\|^2 \tag{11}$$

with W_l the fine scale soil moisture expressed in (10) and TB_G^m the measured SMOS observation. The cost function F is then minimized to invert the couple (W_G, f_1). Note that the problem of retrieving the couple (W_G, f_1) from SMOS data is theoretically well defined because the number of independent SMOS observations contained in TB_G^m is superior to the number of unkonwns, which is two. This statement is a priori true whatever the nature of RT model.

d) Invert W_G: the SMOS scale soil moisture W_G is inverted by setting $f_1 = 0$:

$$W_G^{\text{inv}} = \text{Argmin}_{W_G} F(W_G, 0) \tag{12}$$

with W_G^{inv} the inverted SMOS scale soil moisture.

e) Invert f_1: the contrast parameter f_1 is inverted by fixing $W_G = W_G^{\text{inv}}$:

$$f_1^{\text{inv}} = \text{Argmin}_{f_1} F(W_G^{\text{inv}}, f_1) \tag{13}$$

with f_1^{inv} the inverted contrast parameter of the output distribution. At this point, the soil moisture distribution is entirely determined and is characterized by the couple $(W_G^{\text{inv}}, f_1^{\text{inv}})$. Note that the description given above is the first reading of the method. For an understanding in depth of the different steps of the method, readers are encouraged to refer to Appendix A where the three loops involved in the algorithm are presented.

III. ASSUMPTIONS

In this section, the assumptions implicitely made during the development of the method are listed.

A. Correlation between the radiometric soil temperature and the microwave soil moisture

The correlation between the 1 mm radiometric soil temperature inverted from dual-angle measurement in the thermal infrared and the 0–5 cm L-band soil moisture is the main assumption of the method. In particular, it is assumed that the spatial variations of the 1 mm radiometric soil temperature are linearly correlated with the spatial variations of the integrated 0–5 cm soil temperature. This assumption is required to make the radiometric soil temperature consistent with the 0–5 cm microwave soil moisture [17]. Note that a bias between the radiometric soil temperature and the 0–5 cm soil temperature is expected to have no effect on the disaggregation method because the radiometric soil temperature is only used to provide a relative spatial distribution of the 0–5 cm soil temperature (and therefore of the 0–5 cm microwave soil moisture). In the next, “soil temperature” and “radiometric soil temperature” are alternatively used to refer to the same variable inverted from the thermal infrared. Similarly, “soil moisture” has to be understood in the next sections as the 0–5 cm L-band soil moisture.

B. General assumptions

In the disaggregation method, the general assumptions are:

1) remote sensing data in the visible, near-infrared and thermal infrared are representative of the surface state at the time of SMOS observation. This is particularly important given that SMOS data will be collected at about sunrise and that the optimal conditions for the application of the method occur at about noon when the contrast in soil temperature is generally maximum (high evaporative demand conditions). The synergistic use of SMOS and optical data require therefore that the relative spatial variability of soil moisture within the SMOS pixel does not change much between both observation times. Note that the assumption relies on the relative variability only (not the absolute values of soil moisture) because optical data provide a variability of soil moisture that is relative to the SMOS scale soil moisture.
2) all local auxiliary data have the same spatial characteristics, in particular the same resolution (about 1 km).
3) the same area is monitored by the different view angles of SMOS.
4) disaggregated brightness temperatures correspond approximately to the same set of incidence angles as the set of incidence angles at which the SMOS pixel is observed.

C. Deep soil moisture and temperature

The deep soil moisture W_2 is used by the disaggregation method via LS model to project the soil temperature in (7). As deep soil moisture is generally not known at the scale of 1 km, it is assumed that a rough value can be obtained either with an interpolation technique of in situ measurements or with a SVAT type model. One should note that the accuracy on deep soil moisture is likely to have a negligible effect on the disaggregated soil moisture as the radiometric soil temperature is practically uncorrelated with deep soil moisture [29], [30].

The same assumption is made for the deep soil temperature T_2, which is used by RT model to simulate the local microwave emission in (11).

IV. Application to a Synthetic Scene

In this section, the method is tested with a synthetic scene. We describe first the setup to generate a heterogeneous SMOS pixel. We discuss next about the value of the increment of the contrast parameter δf_1, which is an important task on the algorithmic level. Finally, the results of the application are presented and the validity of the assumption about the correlation soil temperature/soil moisture is first checked.

A. Generate a synthetic scene

Our 40 km size synthetic scene is composed of the ensemble of surface variables and parameters defined at the local scale of 1 km and of the 40 km resolution SMOS observation. The procedure followed to generate a heterogeneous SMOS pixel consists of the following: (1) all independent surface variables and parameters (i.e. all variables except surface component temperatures) are generated within a given range, delimited by a minimal and maximal value; (2) the ensemble of generated surface variables are injected into LS model to compute the value of soil temperature for each sub-pixel; (3) local microwave emissions are simulated with RT model on each sub-pixel; (4) SMOS observation is generated averaging the contribution of each sub-pixel over the SMOS pixel.

Soil moisture is generated with three different ranges: 5–20 %, 10–25 % and 15–30 %. An arbitrary spatial structure is used so that the output distribution can be visually compared to the generated distribution. The spatial structure is the same for the three soil moisture ranges.

LAI and soil texture are generated heterogeneously within the SMOS pixel with an arbitrary spatial structure, independent from each other. We consider that the vegetation cover and the soil texture are the surface variables most important to first check the method as vegetation is involved in both LS and RT model and soil texture parameterizes the relationship soil temperature/soil moisture by conditioning the evaporation rate at the surface soil. Canopy height and vegetation water content are arbitrarily set to 1/6 and 1/2 of LAI respectively as in [38]. The minimum and maximum values of LAI are respectively 0.5 and 3.0. Within the

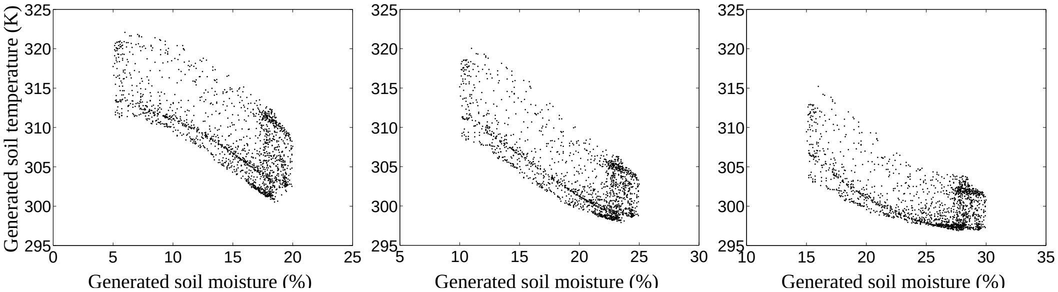

Fig. 4. Radiometric soil temperature generated by LS model as a function of the generated surface soil moisture for three ranges of surface soil moisture: 5–20 %, 10–25 % and 15–30 %. The relationship between radiometric soil temperature and surface soil moisture is made noisy by the spatial variability of LAI. This is a function of soil texture (sand and clay fractions).

synthetic scene, two types of soil texture represented by sand and clay fractions are generated. A sandy soil with 67 % sand and 9 % clay is generated over the left-hand side of the scene and a sandy clay loam soil with 11 % sand and 27 % is generated over the right-hand side. Both types of soil are homogeneous over half a SMOS pixel so that the respective effects of LAI and soil texture on the disaggregated soil moisture can be visually separated.

The heterogeneity of any surface variable other than vegetation and soil texture is expected to have in principle the same effect on the method as the heterogeneity of vegetation: the heterogeneity of any input variable to the LS model will systematically increase the noise in the correlation soil temperature/soil moisture. For the visibility of the results, the surface variables other than LAI and soil texture are therefore set to homogeneous values. The values of air temperature, relative humidity of air, solar radiation, wind speed, deep soil temperature and deep soil moisture are set respectively to 25 C, 20 %, 800 Wm^{-2}, 2 ms^{-1}, 20 C and 20 %.

The variations of the generated soil temperature as function of the generated soil moisture are presented in Fig. 4. One observes that the relationship between soil temperature and soil moisture is made noisy by the heterogeneity of vegetation cover. This is a function of soil texture.

Synthetic SMOS observations are generated by considering two different configurations. In the case of configuration “3 independent TB_G^m”, SMOS observation is composed of the nadir brightness temperature and the horizontal and vertical polarized brightness temperatures with an incidence angle of 40 degrees. In the case of configuration “11 independent TB_G^m” SMOS observation is composed of the nadir brightness temperature and the horizontal and vertical polarized brightness temperatures with an incidence angle of 10, 20, 30, 40 and 50 degrees. Both observation configurations are used to assess the potential of the angular capabilities of SMOS sensor to retrieve $(W_G^{\text{inv}}, f_1^{\text{inv}})$.

B. Sign of the contrast parameter f_1

The disaggregation algorithm increases the contrast parameter f_1 from 0 to an extremal value (see Appendix A for detail) to minimize the cost function $F(W_G^{\text{inv}}, f_1)$. If the absolute value of the increment δf_1 is directly related to the accuracy on the output soil moisture distribution, its sign is imposed by the surface conditions at the time of SMOS observation. In (10) we clearly see that the sign of the contrast parameter depends on the variation of Projected soil temperature with respect to soil moisture. In fact, the slope of the correlation between Projected soil temperature and soil moisture depends on atmospheric conditions. For example, when atmospheric forcing behaves as a thermal energy source towards the surface (high solar radiation in particular), soil temperature is a decreasing function of soil moisture by thermal inertia. Conversely, when atmospheric forcing behaves as a sink of thermal energy towards the surface (usually during the night), soil temperature tends to increase with soil moisture. In the present case where the evaporative demand is high ($S = 800$ Wm^{-2}), Projected soil temperature is a decreasing function of soil moisture. The contrast parameter is therefore negative. In the simulations, the value of the increment δf_1 is set to -0.1.

C. Results

The disaggregation method is applied to three synthetic scenes corresponding to the three ranges of the generated soil moisture. The set of SMOS brightness temperatures used for the present application corresponds to configuration “3 independent TB_G^n”. Note that identical results are obtained with configuration “11 independent TB_G^n” since no noise is added on SMOS observation. In Fig. 5 are presented the images of the disaggregated soil moisture to be compared with the images of the generated soil moisture. For the three soil moisture ranges, the spatial structure of the generated soil moisture is well restored by the disaggregation method and the impact of the heterogeneity of vegetation cover is not detectable on the disaggregated soil moisture. Concerning the heterogeneity of soil texture, the junction between both soil types is slightly apparent on the vertical line at the middle of the images. These qualitative results are also visible in Fig. 6 showing the scatter plots of the disaggregated soil moisture versus the generated soil moisture for the three soil moisture ranges.

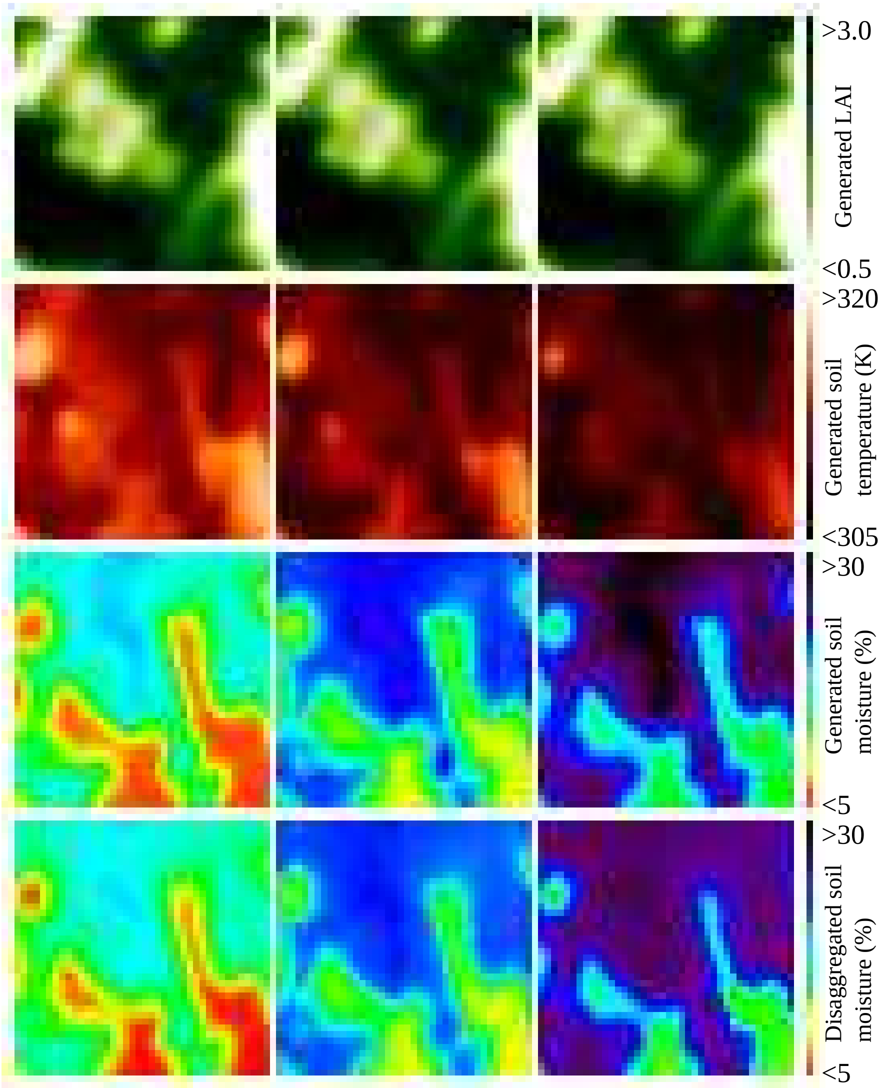

Fig. 5. Images of the main surface variables. Line 1: generated LAI (m^2/m^2); line 2: generated soil temperature (K); line 3: generated soil moisture (%); line 4: soil moisture disaggregated by the method (%). The three columns correspond to three generated soil moisture ranges. Column 1: the generated soil moisture ranges from 5 to 20 %; column 2: from 10 to 25 %; column 3: from 15 to 30 %.

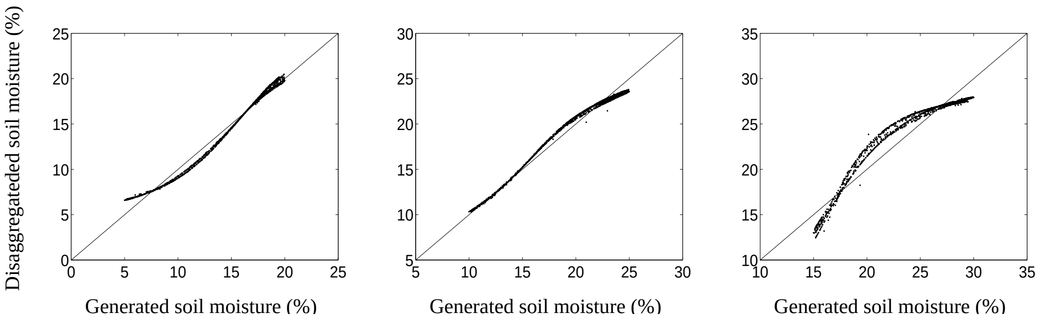

Fig. 6. Soil moisture disaggregated by the method as a function of the generated soil moisture. Three ranges of soil moisture are considered: 5–20 %, 10–25 % and 15–30 %.

TABLE I

RESULTS OF THE OUTPUT DISTRIBUTION IN TERMS OF THE INVERTED SMOS SCALE SOIL MOISTURE W_G^{INV} (%), THE INVERTED CONTRAST PARAMETER f_1^{INV} (%/K) AND THE ERROR SD (%) ON THE DISAGGREGATED SOIL MOISTURE DISTRIBUTION, CORRESPONDING TO 3 DIFFERENT RANGES OF SOIL MOISTURE.

Range of soil moisture	Inverted SMOS scale soil moisture W_G^{inv} (%)	Inverted contrast parameter f_1^{inv} (%/K)	Error on the output distribution SD (%)
5–20 %	14.5	-1.1	0.61
10–25 %	19.5	-1.0	0.56
15–30 %	24.5	-1.6	1.30

The quantitative results in terms of the inverted SMOS scale soil moisture W_G^{inv} (%), the inverted contrast parameter f_1^{inv} (%/K), and the error SD (%) on the ouput distribution computed as the standard deviation between disaggregated and generated values are presented in Table I. We observe that f_1^{inv} has different values for the three ranges of the generated soil moisture. To interpret this result, the variations of Projected soil temperature versus the generated soil moisture are shown in Fig. 7. As observed on the graphs, the slope of the relationship between Projected soil temperature and soil moisture varies with the range of soil moisture and decreases significantly for high values. As a matter of fact, to account for lower sensitivity of Projected soil temperature to soil moisture in the soil moisture range 15–30 %, the algorithm estimates an optimal contrast parameter higher in absolute value (-1.6 %/K) than the one (-1.0 %/K) inverted for the soil moisture range 10–25 %. The same phenomenon is also observed for low soil moisture values. The differences in terms of f_1^{inv} between the different soil moisture ranges are explained by a loss of sensitivity of soil temperature for extreme soil moisture values.

The saturation of Projected soil temperature for low and high soil moisture values represents a limitation of the disaggregation method. As the main assumption relies on the linearity of the variations of Projected soil temperature, the non-linearity of these variations cannot be taken into account by the method. In fact, saturation phenomena imply systematic errors on the disaggregated soil moisture distribution. For example, the error SD is estimated to be 0.6 % for the soil moisture range 10–25 % whereas this quantity is evaluated to be 1.3 % for the soil moisture range 15–30 %, where the assumption of linearity is not as well verified as

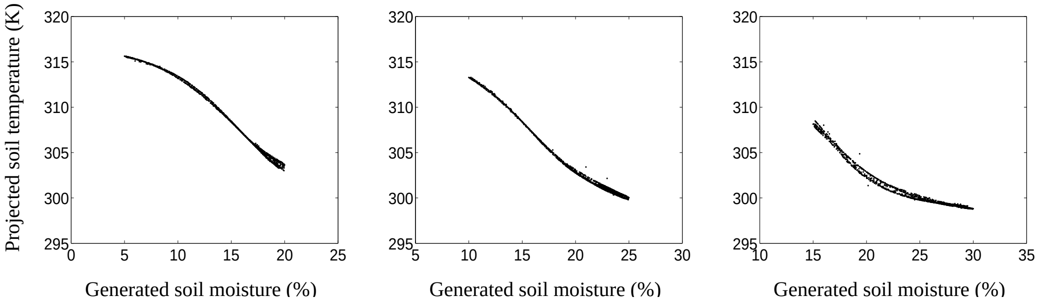

Fig. 7. Projected soil temperature $\overline{T_{sl}^{m}}$ as a function of the generated soil moisture. Three ranges of soil moisture are considered: 5–20 %, 10–25 % and 15–30 %.

for the case 10–25 %. Nevertheless, one should note that the error on the disaggregated soil moisture, which is less than 1.3 % in the conditions of the simulations, is still satisfying.

V. SENSITIVITY

To test the disaggregation method in conditions closer to the operational application, specific uncertainities are generated on the synthetic input dataset. The sensitivity analysis is conducted by adding an increasing gaussian noise separately on fine scale auxiliary data and on SMOS observation. As it is shown in Fig. 3, local auxiliary data provide the information on the spatial variability of soil moisture whereas SMOS observation defines the solvability of the disaggregation problem by inverting the couple $(W_G^{\text{inv}}, f_1^{\text{inv}})$. The synthetic scene used for the sensitivity analysis corresponds to the soil moisture range 10–25 %.

A. Effect of a prescribed noise on local input data

In this subsection, the sensitivity analysis aims to quantify the error on the disaggregated soil moisture that is specifically attributed to the uncertainty in local auxiliary information. Two cases “2 K on T_{sl}^{m} and 20% on LAI_l^{m}” and “4 K on T_{sl}^{m} and 50% on LAI_l^{m}” are considered. They correspond respectively to a gaussian noises of 2 K and 4 K for soil temperature and a gaussian noise of 20 % and 50 % for LAI, evaluated as a percentage of the generated value. The robustness of the disaggregation method is evaluated by computing three parameters: the inverted SMOS scale soil moisture W_G^{inv} (%), the inverted contrast parameter f_1^{inv} (%/K) and the error SD (%) on the ouput distribution computed as the standard deviation between the disaggregated and generated soil moisture. The statistical results computed from 200 independent datasets are presented in Table II in terms of mean and standard deviation

TABLE II

Results of the sensitivity analysis for configurations “3 independent TB_G^m” and “11 independent TB_G^m”. The statistical results are given in terms of mean and standard deviation of the inverted SMOS scale soil moisture W_G^{inv} (%), the inverted contrast parameter f_1^{inv} (%/K) and the error SD (%) on the disaggregated soil moisture distribution.

	Inverted SMOS scale soil moisture W_G^{inv} (%)		Inverted contrast parameter f_1^{inv} (%/K)		Error on the output distribution SD (%)	
Input Noise	3 TB_G^m Mean (SD)	11 TB_G^m Mean (SD)	3 TB_G^m Mean (SD)	11 TB_G^m Mean (SD)	3 TB_G^m Mean (SD)	11 TB_G^m Mean (SD)
No noise	19.5 (0)	19.5 (0)	-1.0 (0)	-1.0 (0)	0.6 (0)	0.6 (0)
2K on $T_{\mathrm{s}l}^m$ 20% on LAI_l^m	19.5 (0.0)	19.5 (0.0)	-1.0 (0.0)	-1.0 (0.0)	1.6 (0.0)	1.6 (0.0)
4K on $T_{\mathrm{s}l}^m$ 50% on LAI_l^m	19.3 (0.1)	19.3 (0.1)	-0.9 (0.2)	-1.0 (0.2)	3.3 (0.3)	3.4 (0.3)
1K on TB_G^m	19.6 (0.3)	19.5 (0.1)	-0.9 (0.72)	-0.9 (0.59)	2.9 (1.1)	2.2 (1.3)
2K on TB_G^m	19.5 (0.5)	19.5 (0.3)	-1.0 (0.73)	-1.0 (0.68)	3.0 (1.0)	2.7 (1.1)
4K on TB_G^m	19.5 (1.0)	19.5 (0.5)	-1.0 (0.75)	-1.0 (0.73)	3.2 (0.9)	2.9 (1.0)

of the three parameters. In the case of configuration “3 independent TB_G^m”, which is a priori less favorable than configuration “11 independent TB_G^m”, and using the data set “4 K on $T_{\mathrm{s}l}^m$ and 50% on LAI_l^m”, which is more noisy than the dataset “2 K on $T_{\mathrm{s}l}^m$ and 20% on LAI_l^m”, the output disaggregated soil moisture is still satisfying in terms of W_G^{inv}, f_1^{inv} and SD. In particular, parameters W_G^{inv} and f_1^{inv} vary not much around the values obtained with non noisy data. The uncertainties in auxiliary data thus transmit a non biased noise to the ouput disaggregated soil moisture and have no impact on the retrievability of both parameters W_G^{inv} and f_1^{inv}. Note that the results obtained for configurations “3 independent TB_G^m” and “11 independent TB_G^m” are statistically the same, which is consistent with the fact that this first sensitivity study deals specifically with local auxiliary data and not with SMOS observation.

B. *Effect of a prescribed noise on SMOS observation*

The second part of the sensitivity analysis is conducted by adding a noise specifically on SMOS observation. Three cases are considered: a noise of 1K, 2K and 4K is successively generated and added on SMOS brightness temperatures for respectively case “1 K on TB_G^m”, "2 K on TB_G^m and "4 K on TB_G^m". Statistical results are given in terms of mean and standard deviation of the three ouput parameters: the inverted SMOS scale soil moisture W_G^{inv} (%), the inverted contrast parameter f_1^{inv} (%/K) and the error SD (%) on the ouput distribution computed as the standard deviation between the disaggregated and generated soil moisture. The statistical results computed from 200 independent datasets are presented in Table II for both configurations "3 independent TB_G^m" and "11 independent TB_G^m". The inverted SMOS scale soil moisture W_G^{inv} is particularly stable whatever the observation configuration. On the other hand, the inverted contrast parameter f_1^{inv} shows important variations around the value obtained with non noisy data (-1.0 %/K). These variations are directly attributed to the uncertainty in SMOS observation. The results corresponding to configuration "11 independent TB_G^m" are better than those of configuration "3 independent TB_G^m" in terms of sensitivity. However, the increase of the number of independent brightness temperatures does not improve significantly the robustness of the inversion process of the contrast parameter. The sensitivity analysis thus shows that the uncertainity in SMOS observation is, in the conditions of the simulations performed, the limiting factor of the disaggregation method.

VI. A SIMPLE APPLICATION TO SGP97/AVHRR DATA

The disaggregation method is now tested with real data. The data collected during the 1997 Southern Great Plains Hydrology Experiment (SGP97) are used synergistically with Advance Very High Resolution Radiometer (AVHRR) channels 1, 2, 4 and 5. In this section, we successively describe the data chosen for the application, we present the two models used to invert the soil temperature from AVHRR data, we describe the methodology followed to extract the spatial variability of soil moisture from AVHRR data and finally we discuss about the results of the disaggregation.

A. The data

Analysis is based on data collected during the 1997 Southern Great Plains Hydrology Experiment (SGP97) run within central Oklahoma between June 18 and July 16, 1997. During SGP97, L-band surface brightness temperature observations were acquired with the Electronically Scanned Thinned Array Radiometer (ESTAR) flown aboard a P3B aircraft. The 800 m brightness temperature imagery was obtained on June 18, 19, 20, 25, 26, 27, 29 and 30, and on July 1, 2, 3, 11, 12, 13, 14, and 16 at around 11:00 CST. The auxiliary data involved in the radiative transfer at L-band –the L-band effective soil temperature, the so-called b parameter, vegetation water content, surface roughness, soil bulk density and soil texture– were gridded [4] at the same resolution as ESTAR brightness temperature. The 0–5 cm soil moisture was then inverted and mapped by [4] at the resolution of 800 m over an area of about 50×200 km^2.

During the SGP97 campaign, NOAA-14/AVHRR overpassed the area almost every day at approximately 14:30 CST. Day July 12 was chosen for the analysis because this day is cloudless and shows the most important range of the soil moisture inverted from ESTAR data over the area covered by both AVHRR and ESTAR observations.

To use AVHRR data synergistically with SGP97 data, the discrepancy between AVHRR and ESTAR resolution is removed by resampling linearly AVHRR data from the actual resolution of 1.1 km to 800 m. The area covered by both ESTAR and AVHRR observations on day July 12 is composed of 3694 sub-pixels at 800 m resolution, which represents an area of about 2400 km^2. In the analysis, this area represents the coarse resolution "SMOS pixel".

Within the SMOS pixel, the available L-band data is the nadir brightness temperature derived from ESTAR data. The point is the disaggregation method presented in the paper requires multiple (at least two) independent brightness temperatures of the same area to calibrate the disaggregated soil moisture (i.e. retrieve the couple $(W_G^{\text{inv}}, f_1^{\text{inv}})$ of the soil moisture distribution). The SMOS angular brightness temperatures used are therefore generated using RT model as in the application with synthetic data: the SMOS angular brightness temperatures are computed averaging the local angular brightness temperatures simulated over each sub-pixel composing the SMOS pixel. The inputs of RT model are the 800 m resolution soil moisture inverted from ESTAR data and the 800 m resolution auxiliary data involved in the radiative transfer at L-band.

Both the radiometric surface temperature T_{rad} and NDVI are derived from AVHRR data. The radiometric surface temperature is estimated using the split-window technique. The equation giving T_{rad} as function of AVHRR channels 4 and 5 is:

$$T_{\text{rad}} = TB^{\text{AVHRR4}} + \frac{TB^{\text{AVHRR4}} - TB^{\text{AVHRR5}}}{\frac{\beta_5}{\beta_4} - 1} + 50\frac{1-\epsilon}{\epsilon} \tag{14}$$

where the first two terms are the radiometric surface temperature computed with the split-window technique [39], and the third term is the correction for surface emissivity [40]. In the analysis, the ratio β_5/β_4 is taken to be 1.33 as in [41] and the mean emissivity ϵ in AVHRR channels 4 and 5 is taken to be 0.96. NDVI is derived from the reflectances of AVHRR channels 1 and 2:

$$NDVI = \frac{R^{\text{AVHRR2}} - R^{\text{AVHRR1}}}{R^{\text{AVHRR2}} + R^{\text{AVHRR1}}} \tag{15}$$

The parameters involved in (3) to compute the fractional vegetation cover from NDVI were set respectively to 0 and 0.60 for $NDVI_{\text{min}}$ and $NDVI_{\text{max}}$ and 0.625 for p as in [42]. The images of the fractional vegetation cover and the surface temperature over the area covered by both AVHRR and ESTAR observations on day July 12 are presented in Fig. 8.

B. The methodology

The methodology followed to disaggregate surface soil moisture within the 2400 km^2 SMOS pixel consists of the following: (1) invert the soil temperature from AVHRR data (2) use the AVHRR soil temperature as a tracer of the spatial variability of fine scale soil moisture and (3) calibrate the disaggregated values of soil moisture using the SMOS observation generated with RT model.

The soil temperature T_{s}^{m} is inverted from AVHRR radiometric surface temperature T_{rad}^{m} given AVHRR fractional vegetation cover f_{c}^{m}. Formally, the inverted soil temperature at fine scale is computed as:

$$T_{\text{s}l}^{\ m} = \frac{T_{\text{rad}l}^{\ m} - f_{\text{c}l}^{\ m} T_{\text{c}l}^{\ m}}{1 - f_{\text{c}l}^{\ m}} \tag{16}$$

with $T_{\text{c}l}^{\ m}$ the canopy temperature at the local scale of 800 m. As the canopy temperature is not available with these data, it is roughly approximated to the air temperature. The assumption that the canopy temperature is close to the air temperature is based on the fact that, except for extreme soil water deficit, plants are able to maintain homeostasis by various means [43]. The value of air temperature used in the inversion of the soil temperature is the average of all the in situ measurements available within the SMOS pixel at the time of AVHRR overpass.

Next, a relative soil moisture distribution is obtained by linking fine scale soil moisture to the inverted soil temperature as:

$$W_l = W_G + f_1 (T_{\text{s}l}^{\ m} - < T_{\text{s}l}^{\ m} >) \tag{17}$$

with W_G the SMOS scale soil moisture and f_1 the contrast parameter fixing the range covered by disaggregated values.

Finally, the relative soil moisture distribution of (17) is normalized at SMOS scale using the generated SMOS observation. This implies the inversion of the SMOS scale soil moisture W_G^{inv} and the contrast parameter f_1^{inv} as described in the development of the disaggregation method (Section II).

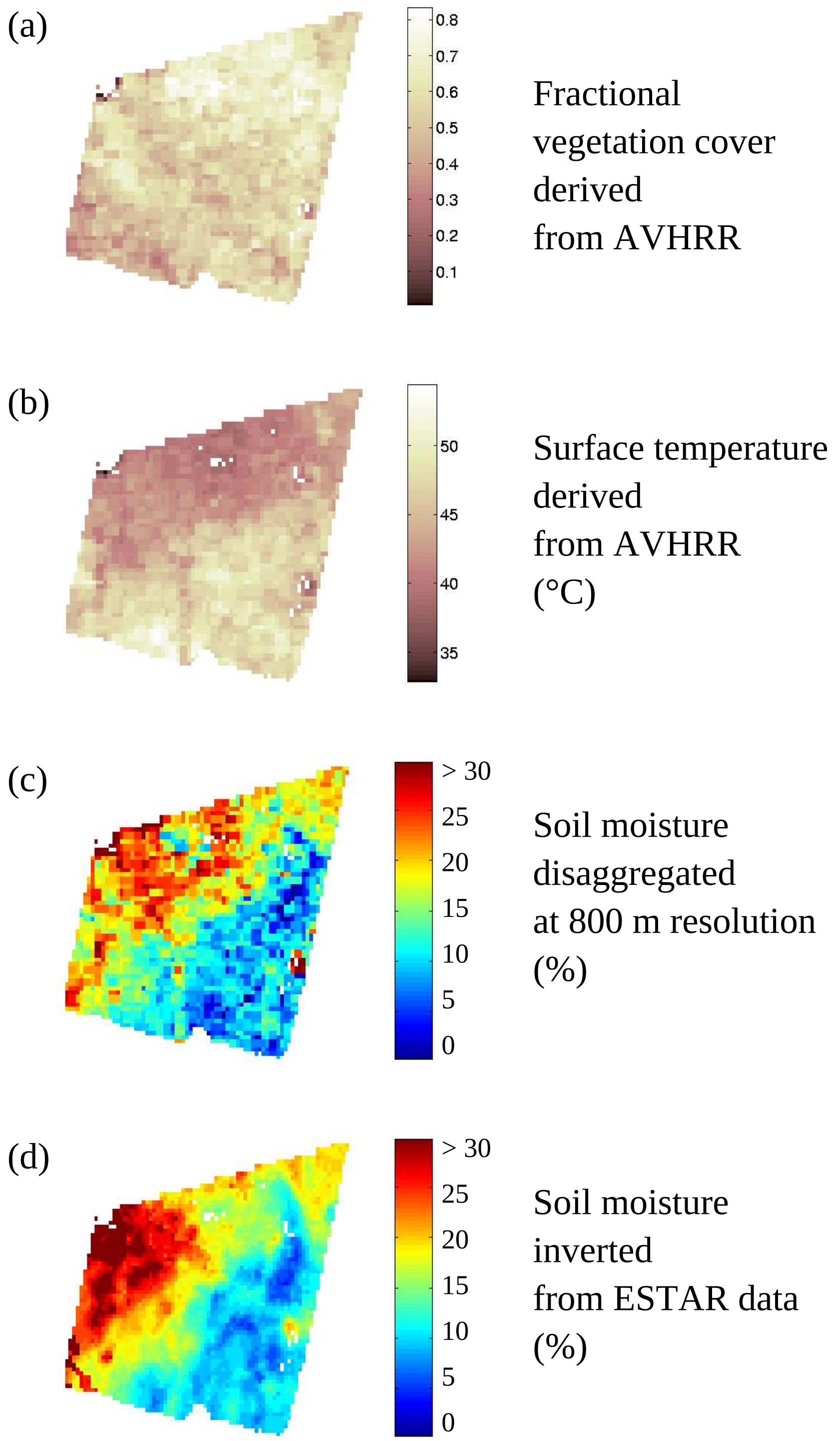

Fig. 8. Images within the 2400 km^2 SMOS pixel of (a) the fractional vegetation cover (m^2/m^2) derived from AVHRR channels 1 and 2, (b) the surface temperature (C) derived from AVHRR channels 4 and 5, (c) the soil moisture (%) disaggregated by the method and (d) the soil moisture (%) inverted from ESTAR data.

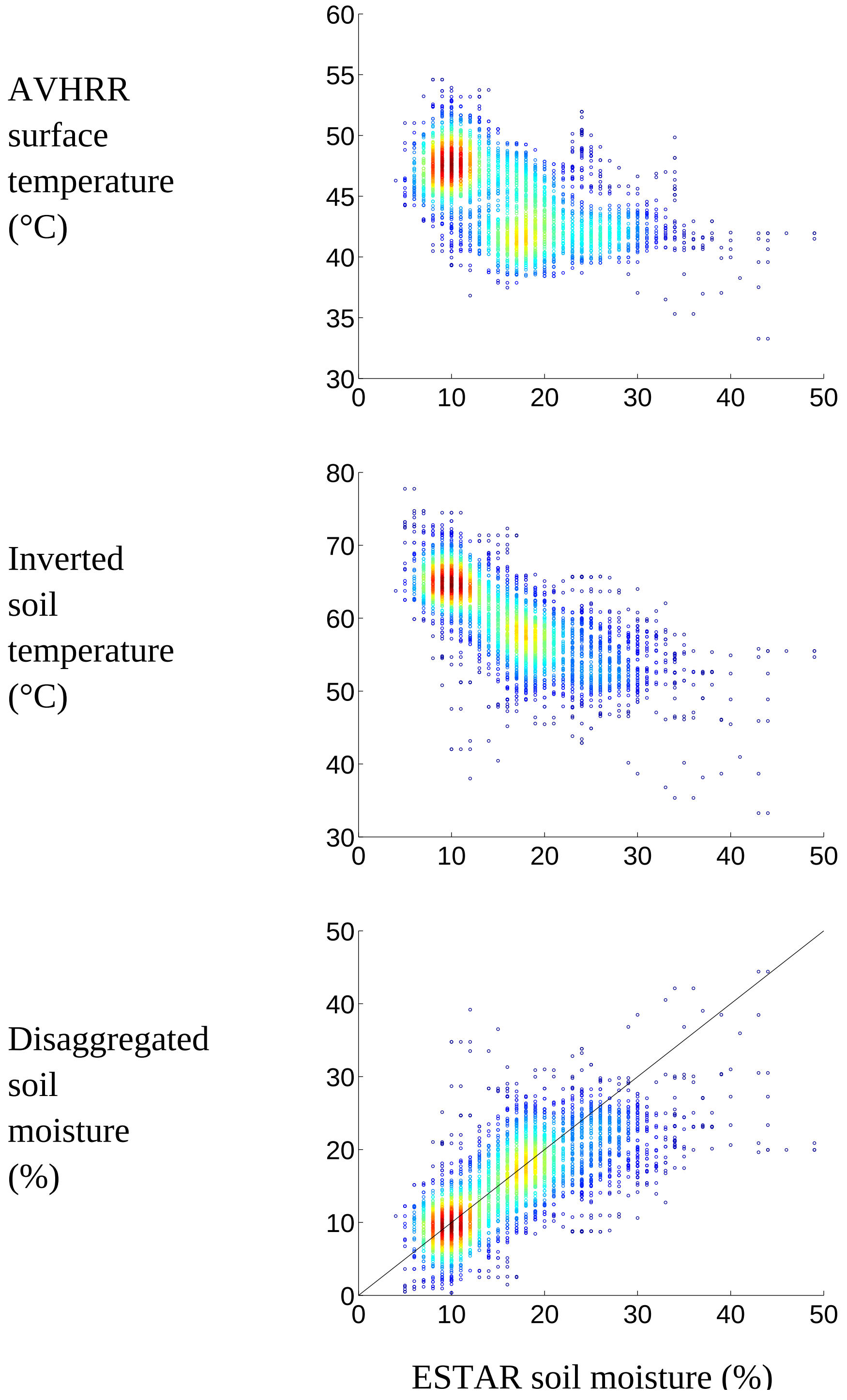

Fig. 9. Surface temperature (C), the inverted soil temperature (C) and the disaggregated soil moisture (%) are ploted as function of ESTAR soil moisture (%). The comparison between the two first plots shows that the soil temperature is a better tracer of ESTAR soil moisture than the surface temperature. In the third plot, the standard deviation between the disaggregated soil moisture and ESTAR soil moisture is found to be 4.0% for 90% of the sub-pixels contained in the SMOS pixel.

C. Results and discussion

The disaggregation method is applied to the 2400 km^2 SMOS pixel generated with SGP97 data. The input data are composed of the surface temperature derived from AVHRR channels 4 and 5, the fractional vegetation cover derived from AVHRR channels 1 and 2 and the SMOS observation generated with RT model from SGP97 data. The output soil moisture distribution is then compared to the soil moisture inverted from ESTAR measurements.

In Fig. 8 are presented the images of the soil moisture disaggregated by the method and the soil moisture inverted from ESTAR measurements. The overall spatial variability of ESTAR soil moisture is well reproduced. The standard deviation between the disaggregated and ESTAR soil moisture is found to be 5.4%, and is better than 4.0% for more than 90% of the 3694 sub-pixels contained in the SMOS pixel. This result is consistent with the uncertainity on the soil moisture inverted from ESTAR data, which was estimated to be about 3% by [4].

The two parameters of the soil moisture distribution were found to be respectively 15.0 % for the SMOS scale soil moisture W_G^{inv} and -1.1 %/K for the contrast parameter f_1^{inv}. Note that the value of the contrast parameter is close to the values that were found with synthetic data in Section IV.

In Fig. 9 are plotted the variations of the disaggregated soil moisture as function of ESTAR soil moisture. We observe that the variability of soil moisture is not as well predicted for high soil moisture values (above 23 %) as for values below 23 %. Quantitatively, the standard deviation between the disaggregated and ESTAR soil moisture is found to be 4.3 % for a range of ESTAR soil moisture limited by a maximum value of 23 %, whereas this quantity is evaluated to be 8.4% for a range of ESTAR soil moisture limited by a minimum value of 23 %. We suggest that the poor results found for soil moisture values above 23 % is due to the non-linearity of the correlation between the soil temperature and the surface soil moisture occuring for high soil moisture values. Indeed the results with synthetic data (Section IV) showed that the saturation of the soil temperature is a limitation of the method.

Even though the spatial variability of fine scale soil moisture is globally well restituted compared to the soil moisture inverted from ESTAR measurements, an important scatter (9.5%) is observed for 10% of the sub-pixels contained in the SMOS pixel. Several additional sources of error could explain this scatter:

1) the soil temperature inverted with RT-TIR model is an approximation of the soil temperature that would be obtained with more complex radiative transfer models.

2) vegetation type is generally not uniform at the scale of 800 m and the proportion of each type is likely to vary within the 2400 km^2 SMOS pixel. As a matter of fact, taking a uniform value for parameter p in (3) may involve errors on the fractional vegetation cover and therefore on the inverted soil temperature.
3) the assumption that the canopy temperature is equal to the air temperature implies errors on the inverted soil temperature.
4) the AVHRR image was georeferenced with a precision estimated to be about 1 km, which is not accurate compared to the resolution of ESTAR data (800 m).
5) AVHRR data were resampled linearly from 1.1 km to 800 m, which may involve systematic errors on interpolated data.
6) other surface variables such as soil texture and atmospheric forcing may have a significant effect on the correlation between the bare soil temperature and surface soil moisture. To account for these effects, a solution could be to project the soil temperature as it is shown in the development of the method in Section II. Two reasons justify that the soil temperature was not projected in this simple application. First, the projection of soil temperature requires a land surface model (LS model for example), which needs to be calibrated in space. As the objective of the application with real data is to give a simple illustration of the disaggregation method, the calibration of LS model over the study area is out of the scope of the analysis. Second, the results of the analysis show that for SGP97 data, the soil temperature is sufficiently well correlated to ESTAR soil moisture to give relatively good estimates of the disaggregated soil moisture.

VII. SUMMARY AND CONCLUSION

In this paper, a new physically-based disaggregation method was developed to improve the spatial resolution of the surface soil moisture extracted from SMOS. The approach is based on an original combination of the 40 km resolution SMOS multi-angular brightness temperatures and 1 km resolution auxiliary data composed of visible, near-infrared and thermal infrared remote sensing data and all the surface variables involved in the modeling of land surface-atmosphere interaction available at this scale (soil texture, atmospheric forcing, etc.). The approach for disaggregating SMOS soil moisture involves two steps. First, the disaggregated soil moisture is expressed as function of the radiometric soil temperature derived from fine scale auxiliary data, and two parameters defined at SMOS scale. The two parameters are the SMOS scale soil moisture W_G and a parameter f_1, called the contrast parameter of the distribution, fixing the range covered by disaggregated values. The second step consists of inverting the couple $(W_G^{\mathrm{inv}}, f_1^{\mathrm{inv}})$ from SMOS data.

The basis of the disaggregation strategy is the correlation between the radiometric soil temperature inverted from the thermal infrared and the microwave soil moisture. To first check the usefullness of this correlation, the method was applied to a synthetic scene representing a heterogeneous SMOS pixel. The results in terms of the disaggregated soil moisture showed that the radiometric soil temperature can be used as a tracer of the spatial variability of soil moisture for a wide range of soil moisture. However, it was also found that the saturation of the soil temperature for extreme soil moisture values is a limitation of the method.

To test the disaggregation method in conditions closer to the operational application, specific uncertainities were generated on the synthetic input dataset. The sensitivity analysis was conducted generating a gaussian noise separately on fine scale auxiliary data and on SMOS observation. The results showed that the disaggregation method remains stable for big uncertainities in auxiliary data (up to 4 K on soil temperature and 50% on LAI). They also showed that the uncertainities in SMOS observation is the limiting factor of the method in the conditions considered. The gaussian noise generated on SMOS observation induced important deviations on the inverted contrast parameter f_1^{inv}. Nevertheless, the comparison of two different observation configurations associated with different view angles showed that an increasing number of independent brightness temperatures improves the retrievability of f_1^{inv}.

The disaggregation method was finally applied on SGP97/AVHRR data. A relative soil moisture distribution was expressed by linking at first order fine scale soil moisture to the soil temperature inverted from AVHRR data. The relative distribution was then normalized with a synthetic SMOS observation. The standard deviation between the soil moisture disaggregated by the method and the soil moisture inverted from ESTAR measurements was found to be less than 4.0 % for 90 % of the sub-pixels contained in the SMOS pixel and 5.4 % for all of the sub-pixels.

Most of the results in this paper were based on synthetic data. To fully assess the applicability of the approach, additional data are needed. In particular, the real database of angular L-band brightness temperatures currently in preparation in the scope of the pre-launch study of SMOS, has to be used to fully assess the robustness of the disaggregation strategy.

In regard to the applicability of the method to single-angle HYDROS [44] observations, two results can be anticipated. Single-angle HYDROS observations are in theory sufficient to invert the couple $(W_G^{\text{inv}}, f_1^{\text{inv}})$ because 2 independent brightness temperatures are obtained with polarizations H and V. In practice however, only 2 independent brightness temperatures may be not sufficient for sensitivity reasons. Indeed, the results of the sensitivity analysis of Section V showed that the number of independent brightness temperatures is an important issue when inverting the contrast parameter f_1^{inv}. To overcome this difficulty, the synergy active/passive microwave HYDROS mission has to be used. A possible approach would be to constrain more the contrast parameter with another disaggregation method based on the synergy active/passive microwave as in [16].

APPENDIX A
ALGORITHM

To distribute fine scale soil moisture within a SMOS pixel, the algorithm runs three loops. The contrast parameter f_1 is incremented with loop 1 to find the minimum of the cost function $F(W_G^{\text{inv}}, f_1)$. Loop 2 is run to insure the convergence of the discrete values of F. Loop 3 is run to maintain the aggregated soil moisture value at the level of the inverted SMOS scale soil moisture W_G^{inv}. In this appendix, the three loops are described independently. For a good understanding of the algorithm, one may refer to the diagram of Fig. 10.

A. *Loop 1: increment* f_1 *to minimize* $F(W_G^{\text{inv}}, f_1)$

The algorithm looks for the value of the contrast parameter f_1 that minimizes the cost function $F(W_G^{\text{inv}}, f_1)$ defined in (11). In practice, the algorithm increases f_1 from 0 to an extremal value and computes the associated values of F. The extremal value of f_1 is defined as the value from which one soil moisture value becomes negative. The output soil moisture distribution is then such as f_1 is optimal with respect to the associated simulated SMOS observation. An illustration of the inversion of f_1^{inv} is provided in Appendix B.

B. *Loop 2: insure the convergence of the iterative values of* $F(W_G^{\text{inv}}, f_1)$

Given a fixed value of f_1, the algorithm computes an associated value of $F(W_G^{\text{inv}}, f_1)$. The point is that the computation of F requires an initialization of the soil moisture distribution W_l. It is reminded that the computation of Projected soil temperature in (7) requires an a priori estimation of fine scale soil moisture. Therefore, the disaggregated soil moisture W_l expressed in (10) and the cost function $F(W_G^{\text{inv}}, f_1)$ depend on the initial values of W_l. A

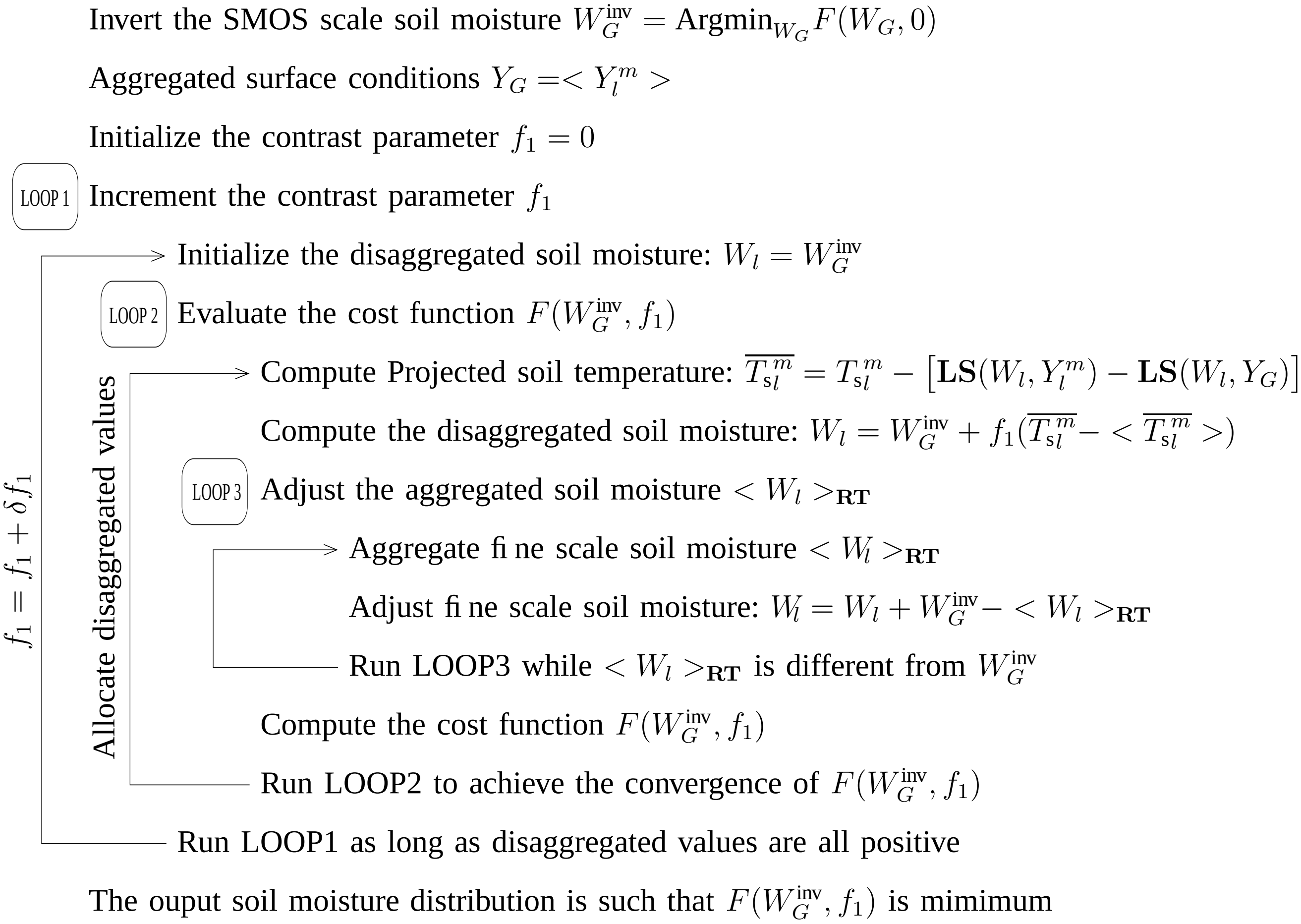

```
Invert the SMOS scale soil moisture $W_G^{\text{inv}} = \text{Argmin}_{W_G} F(W_G, 0)$
Aggregated surface conditions $Y_G =< Y_l^m >$
Initialize the contrast parameter $f_1 = 0$
LOOP 1 Increment the contrast parameter $f_1$
    Initialize the disaggregated soil moisture: $W_l = W_G^{\text{inv}}$
    LOOP 2 Evaluate the cost function $F(W_G^{\text{inv}}, f_1)$
        Compute Projected soil temperature: $\overline{T_{sl}^m} = T_{sl}^m - \left[\mathbf{LS}(W_l, Y_l^m) - \mathbf{LS}(W_l, Y_G)\right]$
        Compute the disaggregated soil moisture: $W_l = W_G^{\text{inv}} + f_1(\overline{T_{sl}^m} - < \overline{T_{sl}^m} >)$
        LOOP 3 Adjust the aggregated soil moisture $< W_l >_{\mathbf{RT}}$
            Aggregate fine scale soil moisture $< W_l >_{\mathbf{RT}}$
            Adjust fine scale soil moisture: $W_l = W_l + W_G^{\text{inv}} - < W_l >_{\mathbf{RT}}$
            Run LOOP3 while $< W_l >_{\mathbf{RT}}$ is different from $W_G^{\text{inv}}$
        Compute the cost function $F(W_G^{\text{inv}}, f_1)$
        Run LOOP2 to achieve the convergence of $F(W_G^{\text{inv}}, f_1)$
    Run LOOP1 as long as disaggregated values are all positive
The ouput soil moisture distribution is such that $F(W_G^{\text{inv}}, f_1)$ is mimimum
```

Fig. 10. Schematic diagram representing the three loops of the algorithm. Loop 1 is run to increment the contrast parameter from an initial value 0 to the extremal value. Given a fixed value of the contrast parameter, loop 2 is run to compute the corresponding value of the global cost function. Loop 3 is run to maintain the global level of the soil moisture distribution at the value inverted from SMOS observation.

loop on W_l is hence necessary to achieve the convergence of $F(W_G^{\text{inv}}, f_1)$. Actually, initial soil moisture values are set to the inverted SMOS scale soil moisture W_G^{inv}:

$$W_l = W_G^{\text{inv}} \tag{18}$$

and loop 2 is run as long as the gap between two iterative values of F is above a given threshold. Once the convergence is achieved, the cost function obtained is independent on initialization and is associated with the given value of the contrast parameter.

C. Loop 3: adjust the value of the soil moisture aggregated at SMOS scale

It is reminded that the algorithm estimates a soil moisture distribution with (10) by setting $W_G = W_G^{\text{inv}}$. As RT model is generally nonlinear, the value of the soil moisture aggregated at SMOS scale (i.e. W_G) is generally not equal to the global value inverted with RT model. It follows that equation (10) is valid only when the aggregated soil moisture W_G is manually adjusted to the inverted soil moisture W_G^{inv}. On the algorithmic level, the aggregated soil moisture is adjusted by adjusting the ensemble of disaggregated values as follows:

$$W_l^{\text{after}} = W_l^{\text{before}} + W_G^{\text{inv}} - < W_l^{\text{before}} >_{\mathbf{RT}} \tag{19}$$

with W_l^{before} the disaggregated soil moisture before adjustment, W_l^{after} the disaggregated soil moisture after adjustment and $< W_l >_{\mathbf{RT}}$ the soil moisture value aggregated in the sense of RT model as:

$$< W_l >_{\mathbf{RT}} = \text{Argmin}_{W_G} \left\| \frac{1}{N} \sum_{l=1}^{N} \mathbf{RT}(W_G, X_l^m) - \mathbf{RT}(W_l, X_l^m) \right\|^2 \tag{20}$$

Loop 3 is run on the aggregated soil moisture $W_G =< W_l >_{\mathbf{RT}}$ as long as the gap between $< W_l >_{\mathbf{RT}}$ and W_G^{inv} is above a given threshold. Note that $< W_l >_{\mathbf{RT}}$ is a priori different from W_G^{inv} because the second term of the norm in (20) is different from TB_G^m.

APPENDIX B

ILLUSTRATION OF THE INVERSION PROCESS

As described in Appendix A, the algorithm inverts the SMOS scale soil moisture W_G^{inv} at the beginning of the scheme. Next, the contrast parameter f_1 is incremented to find the minimum value of the cost function $F(W_G^{\text{inv}}, f_1)$ in an acceptable range of f_1. The values of f_1 parameter should be negative (with the atmospheric conditions considered in Sections IV, V and VI, soil temperature is a decreasing function of soil moisture) and should not exceed the extreme value for which at least one value of the disaggregated soil moisture becomes negative. We provide an illustration of the inversion process of the contrast parameter f_1. In Fig. 11 are presented the variations of the normalized global cost function for different values of the contrast parameter. The simulation is performed with the synthetic data generated in Section IV with the soil moisture range 10–25 % and with an increment of the contrast parameter equal to -0.1. The normalized cost function F_{norm} is defined as:

$$F_{\text{norm}}(W_G^{\text{inv}}, f_1) = \frac{F(W_G^{\text{inv}}, f_1) - F_{\text{min}}}{F_{\text{min}}} \tag{21}$$

with F_{min} the minimum value of F obtained for the optimal value of the contrast parameter f_1^{inv}. In our example, the value of the inverted contrast parameter is found to be -1.0 %/K.

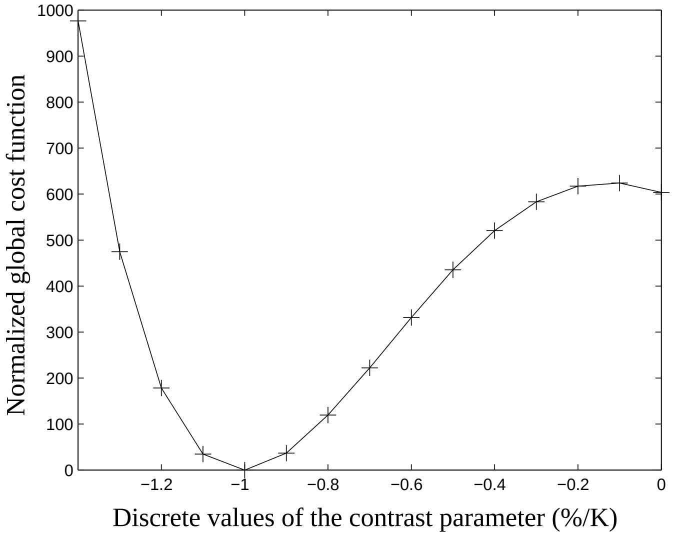

Fig. 11. The minimal value of the global cost function corresponds to $f_1 = -1.0$ %/K.

REFERENCES

[1] J. R. Wang, J. C. Shiue, T. J. Schmugge, and E. T. Engman, "The L-band PBMR measurements of surface soil moisture in FIFE," *IEEE Trans. Geosci. Remote Sensing*, vol. 28, pp. 906–913, september 1990.

[2] T. J. Jackson, D. M. L. Vine, C. T. Swift, T. J. Schmugge, and F. R. Schiebe, "Large area mapping of soil moisture using the ESTAR passive microwave radiometer in Washita '92," *Remote Sens. Environ.*, vol. 53, pp. 27–37, 1995.

[3] T. J. Schmugge, "Applications of passive microwave observations of surface soil moisture," *J. Hydrol.*, vol. 212-213, pp. 188–197, 1998.

[4] T. J. Jackson, D. M. L. Vine, A. Y. Hsu, A. Oldak, P. J. Starks, C. T. Swift, J. D. Isham, and M. Haken, "Soil moisture mapping at regional scales using microwave radiometry: The Southern Great Plains Hydrology Experiment," *IEEE Trans. Geosci. Remote Sensing*, vol. 37, no. 5, pp. 2136–2151, september 1999.

[5] Y. H. Kerr, P. Waldteufel, J.-P. Wigneron, J.-M. Martinuzzi, J. Font, and M. Berger, "Soil moisture retrieval from space: the Soil Moisture and Ocean Salinity (SMOS) mission," *IEEE Trans. Geosci. Remote Sensing*, vol. 39, pp. 1729–1735, august 2001.

[6] J.-P. Wigneron, P. Waldteufel, A. Chanzy, J.-C. Calvet, and Y. Kerr, "Two-dimensional microwave interferometer retrieval capabilities over land surfaces (SMOS mission)," *Remote Sens. Environ.*, vol. 73, pp. 270–282, 2000.

[7] E. T. Engman, "Applications of microwave remote sensing of soil moisture for water resources and agriculture," *Remote Sens. Environ.*, vol. 35, pp. 213–226, 1991.

[8] D. Entekhabi and P. S. Eagleson, "Land surface hydrology parameterization for atmospheric general circulation models including subgrid scale spatial variability," *J. Clim.*, vol. 2, pp. 816–831, 1989.

[9] J. S. Famiglietti and E. F. Wood, "Effects of spatial variability and scale on areally averaged evapotranspiration," *Water Resour. Res.*, vol. 31, no. 3, pp. 699–712, 1995.

[10] E. F. Wood, "Effects of soil moisture aggregation on surface evaporation fluxes," *J. Hydrol.*, vol. 190, pp. 397–412, 1997.

[11] W. T. Crow, E. F. Wood, and R. Dubayah, "Potential for downscaling soil moisture maps derived from spaceborne imaging radar data," *J. Geophys. Res.*, vol. 105, pp. 2203–2212, january 2000.

[12] J. Pellenq, J. Kalma, G. Boulet, G.-M. Saulnier, S. Wooldridge, Y. Kerr, and A. Chehbouni, "A disaggregation scheme for soil moisture based on topography and soil depth," *J. Hydrol.*, vol. 276, pp. 112–127, may 2003.

[13] G. Kim and A. P. Barros, "Space-time characterization of soil moisture from passive microwave remotely sensed imagery and ancillary data," *Remote Sens. Environ.*, vol. 81, pp. 393–403, 2002a.

[14] ——, "Downscaling of remotely sensed soil moisture with a modified fractal interpolation method using contraction mapping and ancillary data," *Remote Sens. Environ.*, vol. 83, pp. 400–413, 2002b.

[15] R. H. Reichle, D. Entekhabi, and D. B. McLaughlin, "Downscaling of radio brightness measurements for soil moisture estimation: A four-dimensional variational data assimilation approach," *Water Resour. Res.*, vol. 37, no. 9, pp. 2353–2364, Sept. 2001.

[16] R. Bindlish and A. P. Barros, "Subpixel variability of remotely sensed soil moisture: An inter-comparison study of SAR and ESTAR," *IEEE Trans. Geosci. Remote Sensing*, vol. 40, pp. 326–337, Feb. 2002.

[17] N. S. Chauhan, S. Miller, and P. Ardanuy, "Spaceborne soil moisture estimation at high resolution: a microwave-optical/IR synergistic approach," *Int. J. Remote Sens.*, vol. 24, no. 22, pp. 4599–4622, 2003.

[18] T. Mo, B. J. Choudhury, T. J. Schmugge, J. R. Wang, and T. J. Jackson, "A model for microwave emission from vegetation-covered fields," *J. Geophys. Res.*, vol. 87, no. 13, pp. 11 229–11 237, 1982.

[19] D. R. Brunfeldt and F. T. Ulaby, "Measured microwave emission and scattering in vegetation canopies," *IEEE Trans. Geosci. Remote Sensing*, vol. 22, pp. 520–524, 1984.

[20] F. T. Ulaby, R. K. Moore, and A. K. Fung, *Microwave Remote Sensing - Active and Passive*. Norwood, MA: Artech House, 1986, vol. 3.

[21] J.-P. Wigneron, L. Laguerre, and Y. Kerr, "A simple parameterization of the L-band microwave emission from rough agricultural soils," *IEEE Trans. Geosci. Remote Sensing*, vol. 39, no. 8, pp. 1697–1707, august 2001.

[22] M. C. Dobson, F. T. Ulaby, M. T. Allinkainen, and M. A. El-Reyes, "Microwave dielectric behavior of wet soil–part ii: Dielectric mixing models," *IEEE Trans. Geosci. Remote Sensing*, vol. 23, pp. 35–46, 1985.

[23] J. R. W. B. J. Choudhury, "Remote sensing of soil moisture content over bare field at 1.4 ghz frequency," *J. Geophys. Res.*, vol. 86, pp. 5277–5282, 1981.

[24] T. J. Jackson and T. J. Schmugge, "Vegetation effects on the microwave emission of soils," *Remote Sens. Environ.*, vol. 36, pp. 203–212, 1991.

[25] D. S. Kimes, "Remote sensing of row crop structure and component temperatures using directional radiometric temperatures and inversion techniques," *Remote Sens. Environ.*, vol. 13, pp. 33–55, 1983.

[26] A. D. Matthias, S. R. Yates, R. Zhang, and A. W. Warrick, "Radiant temperatures of sparse plant canopies and soil using IR thermometry," *IEEE Trans. Geosci. Remote Sensing*, vol. 25, pp. 516–519, 1987.

[27] M. J. McGuire, L. G. Balick, J. A. Smith, and B. A. Hutchison, "Modeling directional thermal radiance from a forest canopy," *Remote Sens. Environ.*, vol. 27, pp. 169–186, 1989.

[28] C. Francois, C. Ottle, and L. Prevot, "Analytical parameterization of canopy directional in the thermal infrared. Application on the retrieval of soil and foliage temperatures using two directional measurements," *Int. J. Remote Sens.*, vol. 12, pp. 2587–2621, 1997.

[29] A. Chehbouni, Y. Nouvellon, Y. H. Kerr, M. S. Moran, C. Watts, L. Prevot, D. C. Goodrich, and S. Rambal, "Directional effect on radiative surface temperature measurements over a semiarid grassland site," *Remote Sens. Environ.*, vol. 76, pp. 360–372, 2001.

[30] C. Francois, "The potential of directional radiometric temperatures for monitoring soil and leaf temperature and soil moisture status," *Remote Sens. Environ.*, vol. 80, pp. 122–133, 2002.

[31] L. Jia, Z.-L. Li, M. Menenti, Z. Su, W. Verhoef, and Z. Wan, "A practical algorithm to infer soil and foliage component temperatures from bi-angular ATSR-2 data," *Int. J. Remote Sens.*, vol. 24, no. 23, pp. 4739–4760, 2003.

[32] F. Baret, J. P. W. Clevers, and M. D. Stevens, “The robustness of canopy gap fraction estimates from the red and near infrared reflectance. a comparison between approaches for sugar beet canopies,” *Remote Sens. Environ.*, vol. 54, pp. 141–151, 1995.

[33] J.-P. Lhomme, A. Chehbouni, and B. Monteny, “Sensible heat flux-radiometric surface temperature relationship over sparse vegetation: parameterizing kB-1,” *Boundary-Layer Met.*, vol. 97, pp. 431–457, 2000.

[34] W. J. Shuttleworth and J. S. Wallace, “Evaporation from sparse crops - an energy combination theory,” *Q. J. R. Meteorol. Soc.*, vol. 111, pp. 839–855, 1985.

[35] R. B. Clapp and G. M. Hornberger, “Empirical equations for some hydraulic properties,” *Water Resour. Res.*, vol. 14, no. 4, pp. 601–604, august 1978.

[36] J. Noilhan and J.-F. Mahfouf, “The ISBA land surface parameterisation scheme,” *Glob. Planet. Change*, vol. 13, pp. 145–159, 1996.

[37] M. Sivapalan, “Linking hydrologic parameterizations across a range of scales: hillslope to catchment to region,” in *Proc. IAHS’93*, vol. 212, Yokohama, Japan, july 1993, pp. 115–123.

[38] J.-P. Wigneron, A. Chanzy, J.-C. Calvet, A. Olioso, and Y. Kerr, “Modeling approaches to assimilating L-band passive microwave observations over land surfaces,” *J. Geophys. Res.*, vol. 107, pp. 148–227, 2002.

[39] J. C. Price, “Land surface temperature measurements from the split window channels of the NOAA-7 Advanced Very High Resolution Radiometer,” *J. Hydrol.*, vol. 276, pp. 112–127, may 2003.

[40] F. Becker, “The impact of spectral emissivity on the measurement of land surface temperature from a satellite,” *Int. J. Remote Sens.*, vol. 8, pp. 1509–1522, 1987.

[41] A. L. Kaleita and P. Kumar, “AVHRR estimates of surface temperature during the Southern Great Plains 1997 Experiment,” *J. Geophys. Res.*, vol. 105, no. D16, pp. 20 791–20 801, 2000.

[42] A. N. French, T. J. Schmugge, W. P. Kustas, K. L. Brubaker, and J. Prueger, “Surface energy fluxes over El Reno, Oklahoma, using high-resolution remotely sensed data,” *Water Resour. Res.*, vol. 39, no. 6, p. 1164, 2003.

[43] T. N. Carlson, R. R. Gillies, and E. M. Perry, “A method to make use of thermal infrared temperature and NDVI measurements to infer soil water content and fractional vegetation cover,” *Remote Sens. Rev.*, vol. 52, pp. 45–59, 1994.

[44] D. Entekhabi, E. G. Njoku, P. Houser, M. Spencer, T. Doiron, Y. Kim, J. Smith, R. Girard, S. Belair, W. Crow, T. J. Jackson, Y. H. Kerr, J. S. Kimball, R. Koster, K. C. McDonald, P. E. O’Neill, T. Pultz, S. W. Running, J. Shi, E. Wood, and J. van Zyl, “The hydrosphere state (HYDROS) satellite mission: an earth system pathfinder for global mapping of soil moisture and land freeze/thaw,” *IEEE Trans. Geosci. Remote Sensing*, vol. 42, no. 10, pp. 2184–2195, 2004.